Fermi surface and magnetic properties of $Ce_xLa_{1-x}Sb$ alloys ($x=0.5,0.9$)

Yoshiki Nakanishi,* Takuo Sakon, Fumihiko Takahashi, and Mitsuhiro Motokawa
Institute for Materials Research, Tohoku University, Sendai, 980-8577, Japan

Akihiro Uesawa
Graduate School of Science, Tohoku University, Sendai, 980-8578, Japan

Masato Kubota†
Neutron Scattering Laboratory, I.S.S.P., University of Tokyo, Tokai, Ibaraki 319-1106, Japan

Takashi Suzuki
Institute for Solid State Physics, University of Tokyo, Tokyo 106-8666, Japan

We have investigated the Fermi surface (FS) and magnetic properties of $Ce_xLa_{1-x}Sb$ alloys for $x=0.9,0.5$ by means of the de Haas–van Alphen effect and high-field magnetization measurements. We successfully observed quantum oscillations in $Ce_{0.5}La_{0.5}Sb$ and determined its Fermi surface. The other missing α FS due to the p-f mixing effect in $Ce_xLa_{1-x}Sb$ at high concentration, which degenerates for spins in LaSb at the X_z point, was found in $Ce_{0.5}La_{0.5}Sb$. The obtained results indicate that the FS and magnetic properties of $Ce_xLa_{1-x}Sb$ exhibit a remarkable transformation, strongly dependent on La substitution due to the suppression of the p-f mixing effect. These results indicate that the p-f mixing effect becomes weaker and, consequently, the crystalline electric field effect becomes dominant in $Ce_xLa_{1-x}Sb$ with increasing La concentration.

I. INTRODUCTION

Ce monopnictides CeX ($X=P, As, Sb, Bi$) with the NaCl crystal structure have attracted much attention because of its anomalous magnetic and transport properties.[1,2] Especially, CeSb has been studied intensively because of its amazing physical properties. CeSb exhibits a complex magnetic phase diagram where at least 14 different magnetic structures exist depending on the magnetic fields and the temperatures.[3] Since these are the most typical low carrier systems, the Fermi energy occurs in a region of the band structure where such interactions are important as follows: the intra-atomic d-f interaction, interatomic d-f or p-f mixing effect, crystalline electric field (CEF) effect [where d represents the conduction electrons—namely, $5d$ or $6s$ electrons in rare-earth atoms—p represents the p band (holes) of pnictogen]. It is well known that the magnetic properties are due to such indirect exchange interactions in $4f$ electron systems. That is to say, these interactions affect the structure of Fermi surface (FS) and very sensitive to the carrier number. Thus it is expected that slight perturbations, for example, such as magnetic fields or pressures, bring about various magnetic phenomena in such a low-carrier $4f$-electron system. Actually, such anomalous behaviors have been observed by the magnetization and de Haas–van Alphen (dHvA) effect measurement of CeSb.[4–11] In the rare-earth monopnictides, represented by RX ($R=$ rare earth), the conduction band is formed by the $5d$ orbits of the cation R and has its minimum at the X points in the Brillouin zone, while the valence band formed mainly by the anionic np state of X ($n=2,3,4,5$) has its maximum at the Γ point in the Brillouin zone.[6]

Here we review the FS of LaSb and CeSb, briefly.[5,7–11] The FS of LaSb consists of twofold ellipsoidal electron FS's

α at the X points and twofold spherical hole FS's β and twofold octahedral hole FS's γ at the Γ point. Here every twofold FS's degenerate for up and down spins. The α electron FS's correspond to the La $d(t2g)$ character of the conduction bands. The β and γ hole FS's correspond to the mostly Sb $5p$ character ($j=3/2$: $5p$-Γ_8) of the valence bands. On the other hand, the Fermi surface of CeSb in the ferromagnetic phase, which was determined by dHvA effect measurements, can be explained by band structure calculations based on the anisotropic p-f mixing model proposed by Kasuya *et al.*[12] and Sakai *et al.*[13] In the p-f mixing model of CeSb, the anisotropic mixing effect between the $4f$-Γ_8 states and $5p$-Γ_8 bands plays an important role. Due to the p-f mixing, the $4f$ state located below the Fermi level with mostly Γ_8 character is pulled down and the $5p$ bands are pushed up by the bonding-antibonding effect to gain energy. Actually, the CEF levels of Ce^{3+} in CeSb have been proposed: $\Gamma_7(0)-\Gamma_8(37\,\text{K})$.[14] This CEF splitting energy $\Delta = 37\,\text{K}$ is much smaller than the value of $\Delta = 264\,\text{K}$ expected from the data of other rare-earth monoantimonides.[15] According to the dHvA experiments and the band structure calculation of CeSb; the FS's consist of the singlefold ellipsoidal electron FS α at the X_z point, twofold ellipsoidal electron FS's γ which exhibit d-f exchange splitting at the X_x and X_y points (we denote them α_x and α_y, respectively in $Ce_xLa_{1-x}Sb$ in this paper), and four singlefold closed-hole FS's (β_1, β_2, β_3, and β_4) at the Γ point (we denote them β_1, β_2, γ_1, and γ_2, respectively in $Ce_xLa_{1-x}Sb$ in this paper to avoid confusion). For the details of notation, refer to Refs. 16 and 17. The FS α at the X_z point is somewhat smaller than that at X_x and X_y points. The electron FS's arise mostly from the $5d$ bands of Ce, while the hole FS's arise mostly from the $5p$ bands of Sb. The hole β_4 FS can be

explained as arising from the particular valence band which mixes strongly with the $4f|J=5/2, J_z=5/2\rangle$ state and is pushed up due to p-f mixing. The other hole β_1, β_2, and β_3 FS's are ascribed to the valence bands which have a little p-f mixing. This p-f mixing effect causes a quite large magnetic anisotropy in CeSb. Even in a magnetic field up to 15 T along the $\langle 011\rangle$ or $\langle 111\rangle$ direction, the magnetic moment is fixed along the $\langle 001\rangle$ axis.[18] Recent studies of CeSb under high pressure reveal that the p-f mixing is very sensitive to pressure and shows anomalous behaviors.[16,17,19] On the contrary, $Ce_xLa_{1-x}Sb$ alloys give an expansion of the distance between Ce ions and also change the effective number of $4f$ electrons. Therefore, alloying experiments are expected to elucidate these anomalous magnetic properties by suppressing the p-f mixing effect. In this paper, we report the FS and magnetic properties of (Ce, La) Sb alloys by means of the de Haas–van Alphen effect and magnetization measurements to reveal how the complicated system CeSb is transformed to the simple reference metal LaSb with varying Ce concentration x. A Brief Report has been already published in Ref. 20.

II. SAMPLE AND EXPERIMENTAL PROCEDURE

The single crystals of $Ce_xLa_{1-x}Sb$ alloys ($x=0.90$ and 0.50) were prepared by the Bridgman method using Ce (99.99%), La (99.99%), and Sb (99.9999%) in a closed tungsten crucible. Their lattice constants are well fitted by Vegard's law. The details of the sample preparation have been published elsewhere.[21] The dHvA measurements were performed by a standard field modulation technique using a ^{3}He cryostat at temperatures down to 0.5 K and a superconducting magnet in fields up to 15 T. The temperature was changed from 0.5 to 4.2 K by controlling the vapor pressure of helium.

The high-field magnetization (M) measurement was carried out in the fields up to 30 T by using a pulsed-field magnet with a pulse duration of 5 msec and at temperatures down to 0.5 K by using the ^{3}He cryostat. The samples were shaped into thin plates, $0.2\times 3\times 3$ mm^3, to avoid the eddy current effect due to the pulsed magnetic field. The details of the high-field magnetization measurement with pulsed-field magnet have been published elsewhere.[22–24] The magnetization measurements were also carried out by using the vibrating sample magnetometer (VSM) method in fields up to 14 T and at temperatures down to 4.2 K. The detailed magnetic susceptibility was measured by superconducting quantum interference device (SQUID) magnetometer from 1.8 to 300 K.

III. EXPERIMENTAL RESULTS

A. Magnetic properties of $Ce_xLa_{1-x}Sb$

Figure 1 shows the lattice constants a and Néel temperatures T_N versus the concentration of Ce, x, for $Ce_xLa_{1-x}Sb$. The Néel temperature of $Ce_{0.9}La_{0.1}Sb$ and $Ce_{0.5}La_{0.5}Sb$ is 15 and 1.5 K, respectively, deduced from specific heat and magnetic susceptibility measurements.[25] For values of LaSb and CeSb, refer to Ref. 26. Figure 2 shows the typical magnetization (M-H) curves of $Ce_{0.9}La_{0.1}Sb$ for $H\|\langle 001\rangle$ axis at several temperatures measured by the VSM. Clear two -step
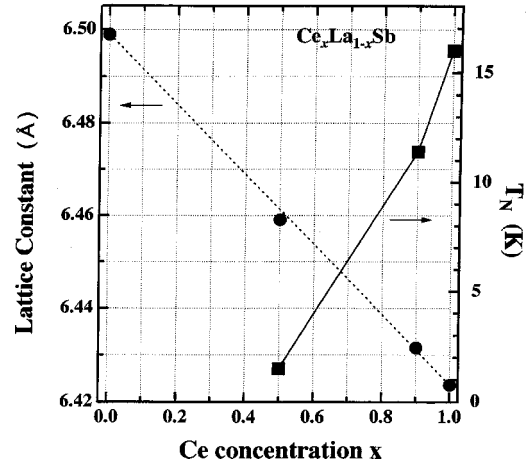
FIG. 1. Variation of the lattice constant a and the Néel temperature vs the Ce concentration x in $Ce_xLa_{1-x}Sb$.

metamagnetic transitions were found at $H_1\sim 2$ T and $H_2\sim 4$ T for $T=4.2$ K accompanied by a hysteresis in which the induced magnetization reaches $1.0\mu_B/Ce$ at H_1 and $2.0\mu_B/Ce$ at H_2. The latter value is mostly equal to the saturated moment for the $|J=5/2, J_z=5/2\rangle$ state, $gJ=2.14\mu_B/Ce$, where g is Lande's g factor and J is the total angular momentum of Ce^{3+}. Besides, another small anomaly was observed at $H_1'\sim 3.8$ T for $T=4.2$ K only with increasing magnetic fields. The first transition H_1 shifts to lower magnetic fields, while the second transition H_2 shifts to higher magnetic fields with increasing temperatures. Both transitions were gradually smeared with increasing temperatures.

Figure 3 shows M-H curves of $Ce_{0.5}La_{0.5}Sb$ for $H\|\langle 001\rangle$, $\langle 011\rangle$, and $\langle 111\rangle$ for $T=0.5$ K measured by the pulsed magnet. A shoulder was found in each principal axis around 4 T. The easy axis of the M-H curves changes from $\langle 001\rangle$ to $\langle 111\rangle$ axis in alloying Ce-LaSb for $x=0.5$. These characteristic features are the same as the previous results reported by Cooper and Vogt.[27] Figure 4 shows the magnetic susceptibility of $Ce_{0.5}La_{0.5}Sb$. It can be explained well taking account of the CEF effect: the CEF energy splitting Δ of 50 K in the
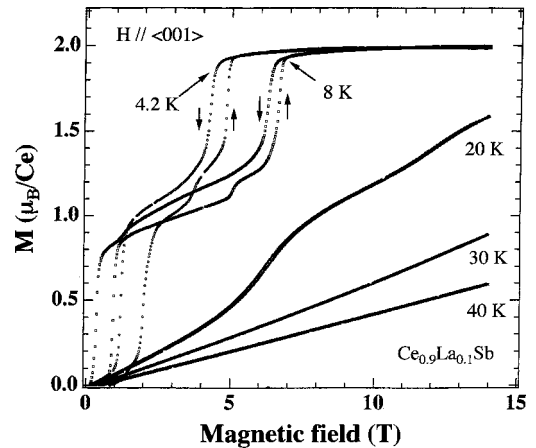
FIG. 2. The magnetization curves of $Ce_{0.9}La_{0.1}Sb$ with fields parallel to the $\langle 001\rangle$ axis at various temperatures.
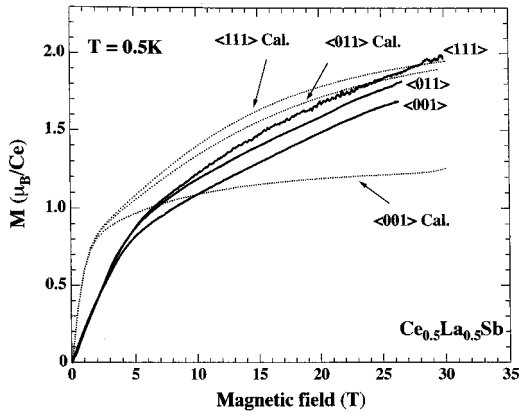
FIG. 3. The magnetization curves of $Ce_{0.5}La_{0.5}Sb$ with fields parallel to the three principal axes at 0.5 K. The dotted line represents the calculated magnetization by the CEF model (inset in Fig. 4) deduced from the result of its susceptibility.

paramagnetic phase, where the CEF ground state is assumed to be Γ_7. The Curie constant was estimated to be 0.85 emu/Ce mol at high temperatures. The effective magnetic moment is estimated to be $2.61\mu_B$/Ce in the paramagnetic phase. This is close to that of the free Ce^{3+} ion, $g\{J(J+1)\}^{1/2} = 2.54\mu_B$/Ce. In Fig. 3 the dotted lines represent the calculated M-H curves by the point-charge CEF model with $\Delta = 50$ K deduced from the magnetic susceptibility measurement. The observed magnetization for $H\|\langle 011\rangle$, $M^{\langle 011\rangle}$ and for $H\|\langle 111\rangle$, $M^{\langle 111\rangle}$, where the superscript denotes the axis along the applied field direction, can be explained well by taking account of the CEF effect with $\Delta = 50$ K. However, the observed $M^{\langle 001\rangle}$ is induced more in high fields than that expected by the proposed CEF model. The prominent feature (the easy axis is $\langle 111\rangle$) can be reproduced by assuming the CEF ground state to be Γ_7 in $Ce_{0.5}La_{0.5}Sb$. This CEF effect indicates that the observed shoulders around 4 T can be ex-
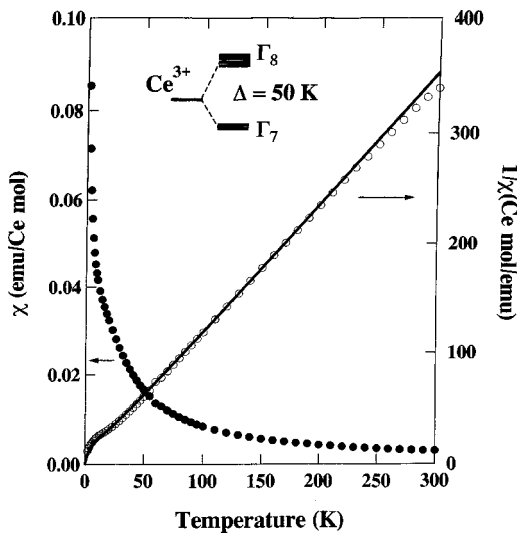
FIG. 4. Temperature dependence of the magnetic susceptibility of $Ce_{0.5}La_{0.5}Sb$. The solid line represents the experimental result. The solid line represents the theoretical inverse susceptibility for the CEF model.
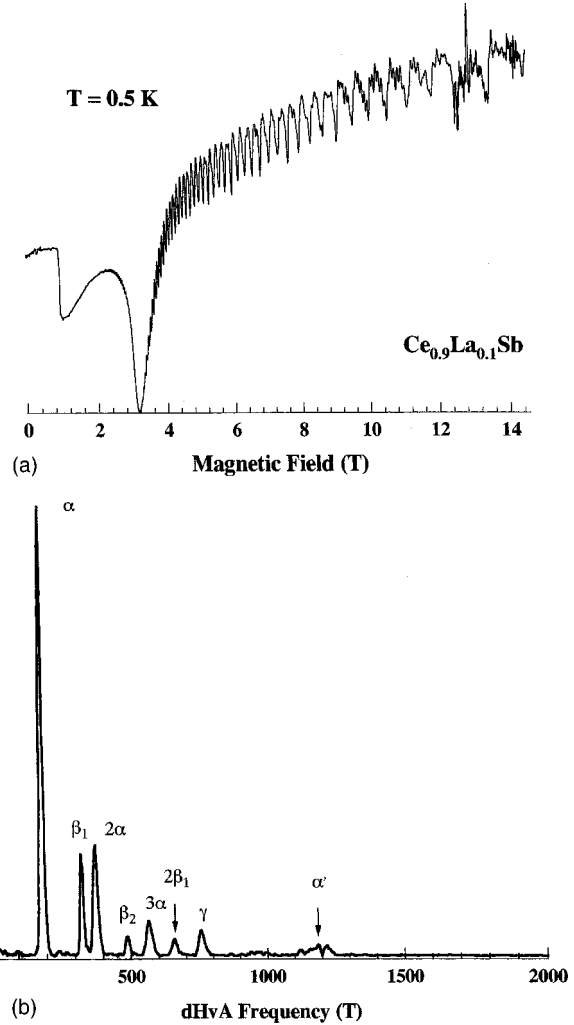
FIG. 5. (a) dHvA signal of $Ce_{0.9}La_{0.1}Sb$ measured at 0.5 K for the field parallel to the $\langle 001\rangle$ axis. (b) The corresponding fast Fourier transform (FFT) spectra in induced ferromagnetic phase.

plained by the fact that the Γ_8 excited state mixes into the Γ_7 ground state to gain the Zeeman energy in magnetic fields.

B. Fermi surface properties of $Ce_xLa_{1-x}Sb$

In this section we report the Fermi surface properties of $Ce_xLa_{1-x}Sb$. Clear quantum oscillations have been observed in both alloys $Ce_xLa_{1-x}Sb$ for $x=0.90$ and 0.50. Figure 5(a) shows the typical dHvA oscillation of $Ce_{0.9}La_{0.1}Sb$ measured at 0.5 K with the field parallel to $\langle 001\rangle$. Two distinct anomalies were observed around 1 and 3 T. They correspond to the phase transitions observed in the present magnetization measurements. Figure 5(b) shows the corresponding fast Fourier transform (FFT) spectra in the field range from 4 to 14 T, which should be the paramagnetic phase [field-induced ferromagnetic phase (IF)]. The angular dependence of the extremal cross-sectional area of FS A_{ext} in the IF phase is shown in Fig. 6. Here we use units of $(2\pi/a)^2$ for the area A_{ext}. One can find that most of the obtained dHvA branches, i.e., FS's, are similar to those of CeSb.[5] We determined all observed branches as indicated by Greek labels in Fig. 6
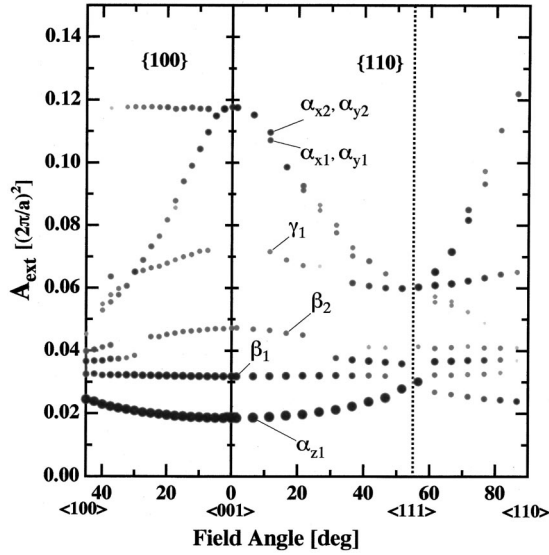
FIG. 6. The angular dependence of the extremal cross-sectional area of FS A_{ext} in the IF phase of $Ce_{0.9}La_{0.1}Sb$.
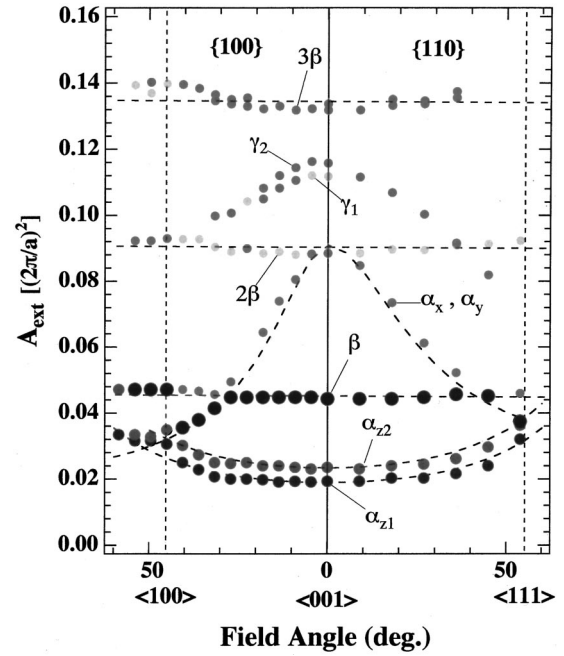
FIG. 8. Angular dependence of the extremal cross-sectional area of FS A_{ext} in the IF phase of $Ce_{0.5}La_{0.5}Sb$. The dotted line represents the calculated results. The α,α' branches are assumed to be three ellipsoids centered at the X points. The β branches are assumed to be a sphere centered at the Γ point.
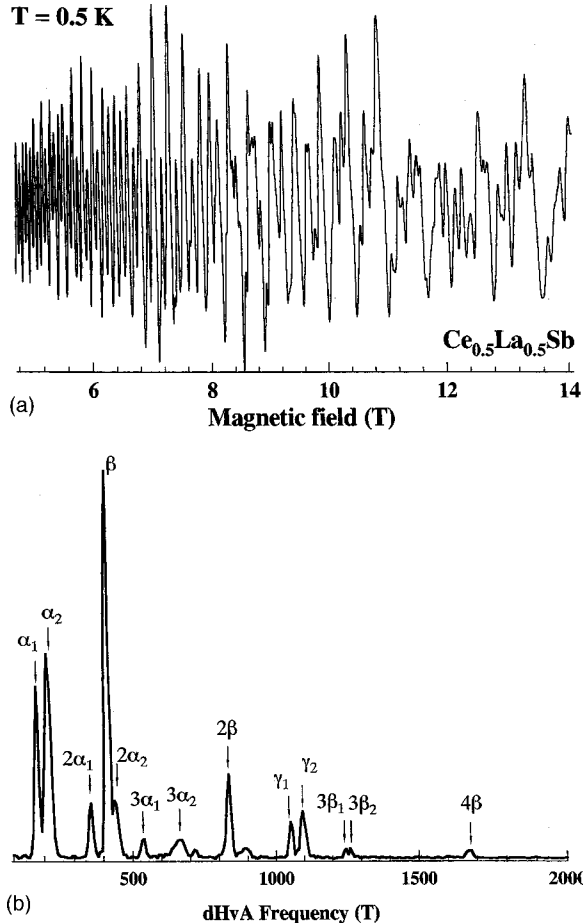
FIG. 7. (a) dHvA signal of $Ce_{0.5}La_{0.5}Sb$ measured at 0.5 K for the field parallel to $\langle 001 \rangle$. (b) The corresponding fast Fourier transform (FFT) spectra in induced ferromagnetic phase.

[ellipsoidal electron FS α at the X_z point α_{z1}, ellipsoidal electron FS's α, which exhibit d-f exchange splitting at the X_x and X_y points α_x and α_y, and four singlefold closed-hole FS's (β_1, β_2, β_3, and β_4) at the Γ point]. Unfortunately, the heaviest branch expected in $Ce_{0.9}La_{0.1}Sb$, which corresponds to β_4 of CeSb, cannot be observed in the present measurement and may be due to the low value of $\omega_c\tau$, where ω_c is the cyclotron frequency and τ is the scattering lifetime of the carrier. The lower temperatures or higher magnetic fields should be necessary to observe it. The magnitude of the spin splittings observed in β and α branches in $Ce_{0.9}La_{0.1}Sb$ become somewhat smaller than those of CeSb as will be discussed later.

Figure 7(a) shows the typical dHvA oscillation of $Ce_{0.5}La_{0.5}Sb$ measured at 0.5 K with the field parallel to $\langle 001 \rangle$. Figure 7(b) shows the corresponding FFT spectra in the field range from 4 to 14 T, which also should be the paramagnetic phase (IF). Figure 8 shows the angular dependence of the extremal cross-sectional area of FS A_{ext} in the IF phase. The most of obtained dHvA branches are similar to those of the reference material LaSb. We determined all observed branches as indicated by Greek labels in Fig. 8 (twofold ellipsoidal electron FS's α at the X point and twofold spherical hole FS's β and twofold octahedral hole FS's γ at the Γ point). However, we have observed spin splittings in the γ branch around the $\langle 001 \rangle$ axis. Furthermore, it is noteworthy that the twofold FS α [the spin splitting of FS α at the X_Z point $(\alpha_{z1}, \alpha_{z2})$] has been observed in $Ce_xLa_{1-x}Sb$ at $x=0.5$, implying α_z to be twofold, which is singlefold in CeSb and $Ce_{0.9}La_{0.1}Sb$. It will be discussed in detail later.

TABLE I. The effective mass of each branch along $\langle 001 \rangle$ axis in $Ce_x La_{1-x} Sb$.

	LaSb	$Ce_{0.5}La_{0.5}Sb$	$Ce_{0.9}La_{0.1}Sb$	CeSb
α branch	0.14[a]	0.14	0.25	0.27[a]
		0.16		
β branch	0.15[a]	0.15	0.48	0.5[a]
			0.68	0.97[a]
γ branch	0.49[a]	0.73	0.82	0.89[a]
				4.3[a]

[a]The effective mass of CeSb and LaSb are taken from Settai *et al.* (Refs. 5 and 26).

The cycrotron mass m_c^* of each branch along the $\langle 001 \rangle$ axis in both $Ce_{0.9}La_{0.1}Sb$ and $Ce_{0.5}La_{0.5}Sb$ is determined by using the conventional method, i.e., by fitting the observed temperature dependence of the amplitude to the Lifshitz-Kosevich formula.[28] The obtained results are summarized in Table I combined with the previous data of CeSb and LaSb reported by the other group.[5,26] All the effective masses of each branch are monotonically lighter, implying the mass enhancement to be reduced with increasing the concentration of La.

Next, we will show the carrier number in $Ce_x La_{1-x} Sb$. First, the volume of each Fermi surface, V_F, is determined by fitting from the obtained angular dependence of the cross-sectional area assumed by the shape of each corresponding Fermi surfaces of LaSb. Then, we can estimate the carrier numbers of each branch, n, from the relation $n = V_F/(4\pi^3)$ without spin degeneracy. The calculated results are summarized in Table II combined with the previous data of CeSb and LaSb reported by the other group.[5,26] Here the carrier number of the γ branch in the parentheses is determined by taking into account the fact that the compound has an equal number of electrons and holes, i.e., $n_e = n_h$, where n_e and n_h denote the number of electrons and holes, respectively. The total carrier number of both the α branch and γ branch is increasing with increasing the concentration of Ce, while the total carrier number of β branch is decreasing with increasing the concentration of Ce.

IV. DISCUSSION

First, we discuss the obtained results of magnetic properties of both $Ce_{0.9}La_{0.1}Sb$ and $Ce_{0.5}La_{0.5}Sb$. As explained in

Introduction, the *p-f* mixing effect plays an important role and is helpful to understand the present results. $Ce_{0.9}La_{0.1}Sb$ exhibits the complicated *M-H* curves mostly similar to those of CeSb, implying the existence of complicated magnetic structures in the fields. In CeSb this complicated magnetic behavior seems to originate in the coexistence of strong in-plane and weak interplane magnetic layers which consist of the occupied $4f$ state of $|J = 5/2, J_z = 5/2\rangle$ with mostly Γ_8 character. Due to the *p-f* mixing, this $4f$ state is considerably pushed down by the bonding-antibonding effect to gain energy in the *x*-rich region. As the present results imply, however, the CEF excited state, which is the occupied $4f$ state of $|J = 5/2, J_z = 5/2\rangle$ with mostly Γ_8 character, seems to shift to higher energy due to the suppression of the *p-f* mixing effect in the $x \sim 0.5$ region: $\Delta(CeSb) = 37$ K,[14] $\Delta(Ce_{0.5}La_{0.5}Sb) = 50$ K. Consequently, *M-H* curves of $Ce_{0.5}La_{0.5}Sb$ exhibit much simpler behaviors compared to those of $Ce_{0.9}La_{0.1}Sb$: The magnetic properties of $Ce_{0.5}La_{0.5}Sb$ seem to be described by the Γ_7 doublet with Kramers degeneracy at lower temperatures, for the behavior of the easy axis of the *M-H* curve may suggest important hints about the *p-f* mixing effect. Actually, the easy axis changes remarkably to the $\langle 111 \rangle$ direction in $Ce_{0.5}La_{0.5}Sb$. We propose the sequence of the CEF model: $\Gamma_7(0)$-$\Gamma_8(50$ K$)$ determined from the magnetic susceptibility. However, this model cannot explain well the $M^{\langle 001 \rangle}$ behavior. At present, we do not have a clear idea. The deviation may be ascribed to a small *p-f* mixing effect even in $Ce_{0.5}La_{0.5}Sb$. Actually, the spin splitting of the γ branch, which is believed to be due to the *p-f* mixing effect, is still observed only along the $\langle 001 \rangle$ axis in $Ce_{0.5}La_{0.5}Sb$. We note that La substitution transforms the magnetic properties remarkably, implying that the *p-f* mixing effect becomes fairly weaker; as a result, the CEF effect can be dominated in the $Ce_x La_{1-x} Sb$ alloy for $x = 0.5$.

Next, we will discuss the obtained results of the FS properties of both $Ce_{0.9}La_{0.1}Sb$ and $Ce_{0.5}La_{0.5}Sb$. As mentioned above, all FS α, β, and γ branches have twofold degenerate sheets for up- and down-spin states in LaSb. However, in CeSb, which has one $4f$ electron in Ce^{3+}, all twofold-degenerate sheets can be split. The spin splitting of the α branch is considered to be due to the intra-*d-f* exchange interaction. Therefore, if in the absence of the *p-f* mixing effect, all α branches at the *X* point would exhibit spin splitting due to intra-*d-f* exchange. Figures 9(a) and 9(b) show the schematic angular dependence of the extremal cross-sectional area of α FS and its schematic electric structure in

TABLE II. The carrier numbers of each branch in $Ce_x La_{1-x} Sb$.

					(numbers/atom)	
	α_z	α_x, α_y	β_1	β_2	γ_1	γ_2
CeSb	0.0024[a]	0.0183[a]	0.0010[a]	0.0015[a]	0.0032[a]	0.0150[a]
$Ce_{0.9}La_{0.1}Sb$	0.0031	0.0171	0.0011	0.0016	(0.0175)	
$Ce_{0.5}La_{0.5}Sb$	0.0024(α_{z1})	0.0105	0.0036		(0.0108)	
	0.0020(α_{z2})					
LaSb		0.014[a]		0.0037[a]	0.010[a]	

[a]The carrier numbers of CeSb and LaSb are taken from Settai (Ref. 26).

(a)

(b)
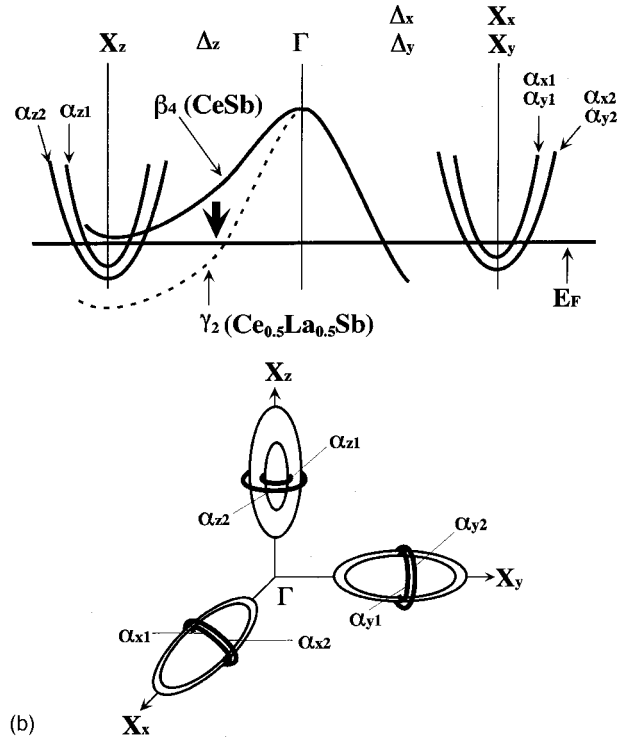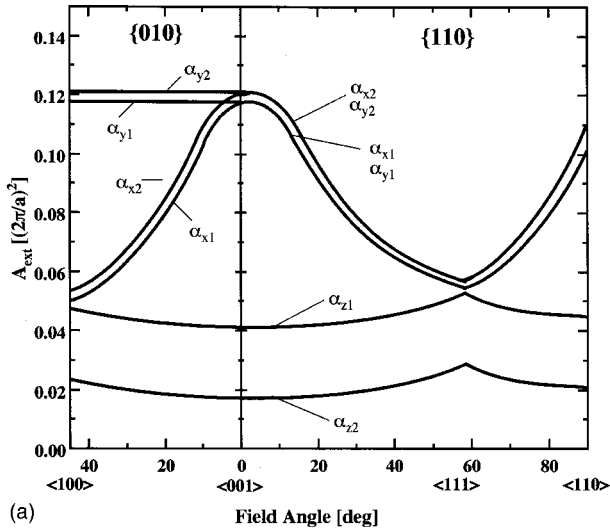
FIG. 9. The schematic angular dependence of the extremal cross-sectional area of ellipsoidal electronic FS α at the X point (a) and its schematic energy band structure in the vicinity of the Γ and X points in k space (b) without the p-f mixing effect represented by a dotted line in the vicinity of the X point. The solid line represents those with the p-f mixing effect.

the vicinity of the Γ point, respectively. These correspond to FS's at the X_x and X_y points observed in $Ce_{0.9}La_{0.1}Sb$ and $Ce_{0.5}La_{0.5}Sb$. However, the behavior of α FS at the X_z points is quite different as affected strongly by the p-f mixing effect. This may be explained as follows. Because of the p-f mixing effect, the $5p$ band corresponding to the β_4 branch is particularly pushed up at the Γ point. The result is hybridization of the $5p$ (β_4 FS) and $5d$ (α_z FS) bands, which is allowed at the X_z point. It was thought that one observed the smaller split-α FS α_{z1} at the X_z point in CeSb as well as

(a)

(b)
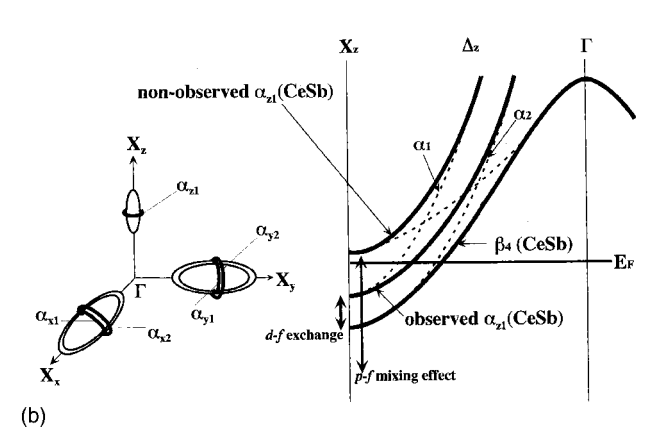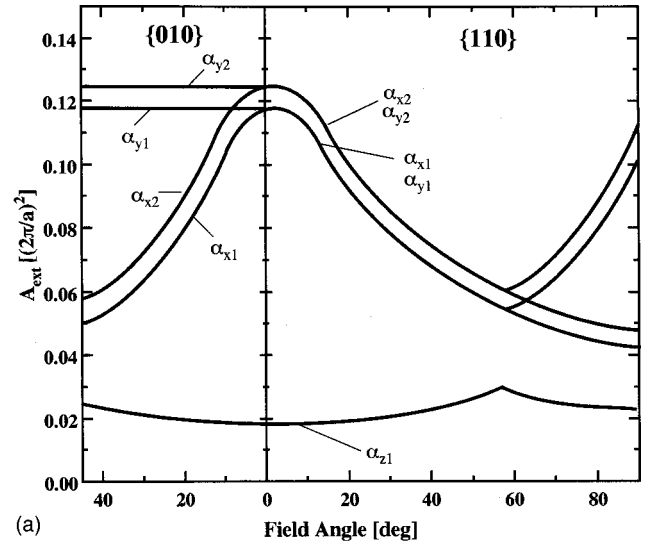
FIG. 10. The schematic angular dependence of the extremal cross-sectional area of ellipsoidal electronic FS α at the X point (a) and its schematic energy band structure in the vicinity of the Γ and X points in k space with the p-f mixing effect. The dotted lines represent the bands before hybridization. After hybridization due to the p-f mixing effect represented by solid lines, one can observe only the smaller α FS (α_{z1}) at the X_z point because the other α FS is pushed up above E_F.

$Ce_{0.9}La_{0.1}Sb$. Figures 10(a) and 10(b) show the schematic angular dependence of this extremal cross-sectional area of α FS and its schematic electric structure in the vicinity of the Γ point, respectively. However, with increasing La substitutions—i.e., the p-f mixing effect is suppressed—the pushed-up $5p$ band returns and α FS which exhibits spin splitting appears at the X_z point. They are most likely to correspond to the observed split-α FS at the X_z point in $Ce_{0.5}La_{0.5}Sb$. These results are in agreement with the predictions of Kasuya *et al.*[12] and Sakai *et al.*[13]

Next, we will discuss the Ce-LaSb alloying dependence of carrier numbers in each FS. The obtained behavior is in agreement with that of FS studies in CeSb under pressure done by Takashita *et al.*[16,17] It revealed that the $5p$ band corresponding to the β_4 branch was particularly pushed up at the Γ point due to the p-f mixing effect. They suggested that with increasing pressure, the p-f mixing effect becomes stronger because the overlap of the wave functions between
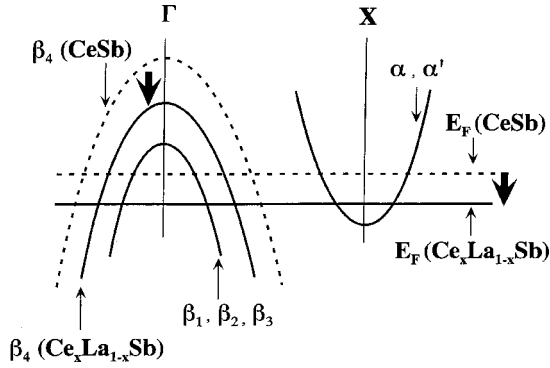
FIG. 11. The schematic energy band structure in the vicinity of the Γ and X points in k space which takes only the p-f mixing effect into account. The solid lines represent the energy bands and the Fermi energy E_F with the weaker p-f mixing effect, while dotted lines represent those with the p-f mixing effect as seen in CeSb.

the $5p$ bands of Sb and the $4f$ states of Ce increases. Therefore, the $5p$ band corresponding to the β_4 branch is particularly pushed up farther at the Γ point with pressure. In the same manner, the Ce-LaSb alloying dependence of carrier numbers in each FS can be explained as follows. The $5p$ band corresponding to the β_4 branch is pushed down at the Γ point with increasing the La concentration due to the suppression of the p-f mixing effect. This effect causes the volume of the β_4 FS to decrease. The Fermi level E_F also decreases to compensate for the numbers of holes and electrons. Consequently, the volumes of the electron FSs decrease, while the volumes of the hole FSs, other than the β_4 FS, increase as shown in Fig. 11. We found a decrease of the effective masses in each branch with respect to the La concentration. This implies that the mass enhancement due to the p-f and d-f many-body interaction is reduced. This also
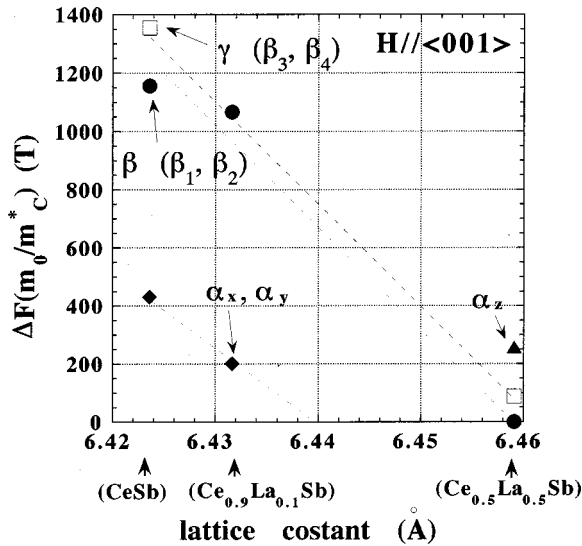
FIG. 12. $(m_0/m_c^*)\Delta F$ for the field along the $\langle 001\rangle$ direction as a function of a lattice constant. The solid squares, solid triangles, solid circles, and open squares denote the values of the $\alpha(\alpha)$, $\alpha(\gamma)$, β, and γ branches, respectively. A description used in the CeSb case is represented in parentheses (Ref. 5).
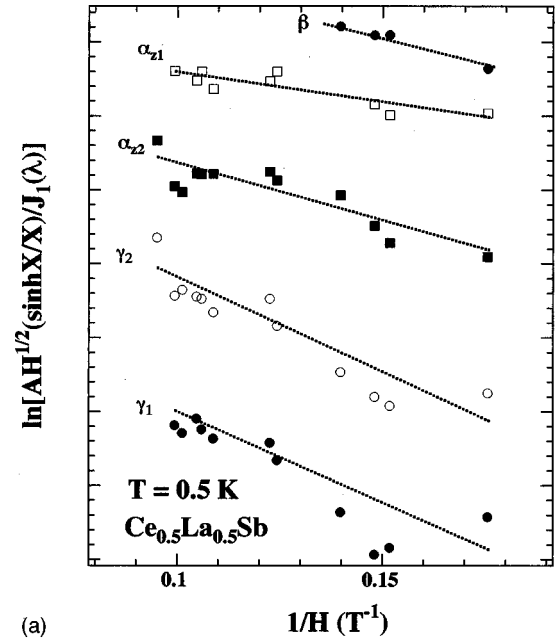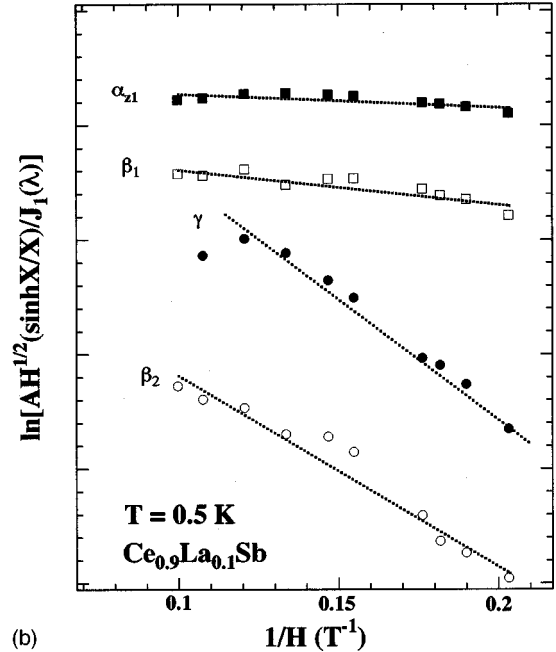
FIG. 13. Dingle plot, the dHvA amplitude A vs inverse magnetic field for the field along the $\langle 001\rangle$ direction at 0.5 K for each branch in $Ce_{0.5}La_{0.5}Sb$ (a) and $Ce_{0.9}La_{0.1}Sb$ (b), respectively, where $X = \xi m_c^* T/H$, $J_1(\lambda)$ is the first-order Bessel function which depends on $\lambda = 2\pi Fh/H^2$. Here h is the modulation field and F is the dHvA frequency.

indicates that the p-f mixing effect becomes weaker in $Ce_xLa_{1-x}Sb$ with increasing the La concentration.

Next, we will comment on the observed spin splittings in $Ce_xLa_{1-x}Sb$ alloys, qualitatively. We can roughly estimate the interaction energy of intra-atomic d-f exchange energy E_{df} and p-f mixing energy E_{pf} by using $E_i \sim (m_0/m_c^*)\Delta F$ assuming the same cyclotron mass for the different spin states, where $\Delta F = |F_\uparrow - F_\downarrow|$ is the difference of the dHvA frequencies with the up- and down- spin states, and i denotes

TABLE III. The dHvA frequency F, Dingle temperature T_D, and corresponding mean free path l of each branch along the $\langle 001 \rangle$ axis in $Ce_xLa_{1-x}Sb$ estimated in Figs. 10(a) and 10(b).

Branch	Ce$_{0.5}$La$_{0.5}$Sb			Ce$_{0.9}$La$_{0.1}$Sb		
	F [T]	T_D [K]	l [Å]	F [T]	T_D [K]	l [Å]
α_1	180	2.76	2690	192	0.32	13400
α_2	216	3.31	2150			
β_1	418	3.71	2850	333	0.43	6860
β_2				497	1.67	1520
γ_1	1053	1.15	3000	762	1.20	2180
γ_2	1096	1.20				

df and *pf*. Figure 12 shows $E_i \sim (m_0/m_c^*)\Delta F$ for the field along the $\langle 001 \rangle$ directions at 8 T, in which the effective field is used as $H = 2(1/H_{p1} + 1/H_{p2})^{-1}$, where H_{p1} and H_{p2} are the end points for the FFT, as a function of a lattice constant. This result indicates that the magnitude of the spin splitting normalized by the each effective mass in any branches seems to be proportional to a concentration of Ce. This suggests that the every interaction energy between localized $4f$ electron and carriers (*p-f* mixing effect, *d-f* exchange interaction) depends considerably on the La substitution.

Finally, we comment on the reason why quantum oscillations can be observed even in the alloying system up to 50% concentration of Ce, Ce$_{0.5}$La$_{0.5}$Sb. In general, the amplitude of quantum oscillations is greatly reduced by even very slight alloying due to a consequence of the extra scattering of electrons by the impurity atoms. Especially, in dHvA oscillations in alloys, they are completely damped out for concentrations of order 1% (atomic) of an impurity component in a pure host.[28] That is to say, in the Ce$_x$La$_{1-x}$Sb alloy system it should be difficult to observe quantum oscillations due to an increase of the Dingle temperature in a conventional understanding of the dHvA effect. However, recently quantum oscillations of Ce$_x$La$_{1-x}$B$_6$ intermetallic for all $0 < x < 1$ were also observed.[29,30] They explain those reasons in detail and agreed with their conclusions that long-lived quasiparticles which consist of all Fermi surfaces may exist even in Ce$_x$La$_{1-x}$Sb for $x = 0.5$. It indicates that the substitution of La by Ce does not cause any significant potential scattering due to charge differences or lattice distortion. The Dingle temperature T_D $[= (\hbar/2\pi k_B)\tau^{-1}]$ or the relaxation time (scattering lifetime) τ is estimated from the field dependence of the amplitude of dHvA oscillations, i.e., from the slope of a plot of $\ln[AH^{1/2}(\sinh X/X)/J_1(\lambda)]$ versus H^{-1} at constant temperature, where A is the dHvA amplitude, X is $2\pi^2 m_c^* c\hbar k_B T/eH$ $(= \xi m_c^* T/H)$, and $J_1(\lambda)$ is the first-order Bessel function which depends on $\lambda = 2\pi Fh/H^2$. Here h

is the modulation field and F is the dHvA frequency. F $[= (c\hbar/2\pi e)S_F]$ is proportional to the extremal cross-sectional area S_F of the Fermi surface. Figures 13(a) and 13(b) show the field dependence of the dHvA amplitude (Dingle plot) for the each branch in $x = 0.5$ and $x = 0.9$, respectively. The effective field is used as $H = 2(1/H_{p1} + 1/H_{p2})^{-1}$. The obtained Dingle temperature and mean free path are listed in Table III. Here, we determined the mean free path l from the relations of the Fermi surface $S_F = \pi k_F^2$, $\hbar k_F = m_c^* \nu_F$, and $l = \nu_F \tau$, where ν_F is the Fermi velocity and k_F is half of the caliper dimension of the Fermi surface S_F. Actually, they indicate that in all cases a higher T_D is approximately 3.7 K (comparable to that in many other pure metals).

V. CONCLUSION

We have performed dHvA effect and high-field magnetization measurements to investigate the magnetic and Fermi surfaces properties of Ce$_x$La$_{1-x}$Sb alloys for $x = 0.9, 0.5$. We determined the topological changes of the FS and changes in effective mass and scattering lifetime of the carrier of Ce$_x$La$_{1-x}$Sb alloys for $x = 0.9, 0.5$. Furthermore, we determined the CEF level scheme in Ce$_{0.5}$La$_{0.5}$Sb alloy. La substitution transforms the dominant-physical effect in the system (from the *p-f* mixing effect to the CEF effect in Ce$_x$La$_{1-x}$Sb alloys) as seen in their FSs and magnetization curves. The band structure around the X_z point was transformed remarkably due to the suppression of the *p-f* mixing effect in the Ce$_{0.5}$La$_{0.5}$Sb alloy. As the result, missing FS due to the *p-f* mixing effect, which is most likely to originate from one of the α branches at the X_z point, have been found in Ce$_{0.5}$La$_{0.5}$Sb. We observed the dHvA signals in the alloying system Ce$_{0.5}$La$_{0.5}$Sb in this compound indicating the existence of long-lived quasiparticles for both the up- and down-spin channels. Our present results support experimentally the anisotropic *p-f* mixing effect.

In order to clarify this fact, further studies, especially theoretical analysis, are necessary. Moreover, the same study of samples with other concentrations may yield important details for qualitative and quantitative discussions.

*Corresponding author. Present address: Department of Materials Science and Engineering, Iwate University, Morioka, 020-8551, Japan. FAX: +81-19-621-6373. Electronic address: yoshiki@iwate-u.ac.jp

†Present address: Photon Factory, Institute of Materials Structure Science, KEK, 1-1 Oho, Tsukuba 305-0801, Japan.

[1] T. Suzuki, Physica B **186−188**, 347 (1993).

[2] P. Wachter, in *Handbook on the Physics and Chemistry of Rare Earths*, edited by K. A. Gschneidner, Jr., L. Eyring, G. H. Lander, and G. R. Choppin (Elsevier, Amsterdam, 1994), Vol. 19, p. 388.

[3] J. Rossat-Mignod, J. M. Effantin, P. Burlet, T. Chattopadhyay, L.

P. Regnault, H. Bartholin, C. Vettier, O. Vogt, D. Ravot, and J. C. Achart, J. Magn. Magn. Mater. **52**, 111 (1985).

[4] G. Busch and O. Vogt, Phys. Lett. **25A**, 449 (1967).

[5] R. Settai, T. Goto, S. Sakatsume, Y. S. Kwon, T. Suzuki, Y. Kaneta, and O. Sakai, J. Phys. Soc. Jpn. **63**, 3026 (1994).

[6] A. Hasegawa, J. Phys. Soc. Jpn. **54**, 677 (1985).

[7] R. Settai, T. Goto, S. Sakatsum, Y. S. Kwon, T. Suzuki, and T. Kasuya, Physica B **186−188**, 176 (1993).

[8] H. Kitazawa, Y. S. Kwon, A. Oyamada, N. Takeda, H. Suzuki, S. Sakatsume, T. Satoh, T. Suzuki, and T. Kasuya, J. Magn. Magn. Mater. **76−78**, 40 (1988).

[9] H. Aoki, G. W. Crabtree, W. Joss, and F. Huliiger, J. Magn. Magn. Mater. **52**, 389 (1985).

[10] H. Kitazawa, T. Suzuki, M. Sera, I. Oguro, A. Yanase, A. Hasegawa, and T. Kasuya, J. Magn. Magn. Mater. **31−34**, 421 (1983).

[11] H. Aoki, G. W. Crabtree, W. Joss, and F. Huliiger, J. Magn. Magn. Mater. **52**, 169 (1991).

[12] T. Kasuya, O. Sakai, J. Tanaka, H. Kitazawa, and T. Suzuki, J. Magn. Magn. Mater. **63−64**, 9 (1987).

[13] O. Sakai, M. Takegahara, H. Harima, K. Otaki, and T. Kasuya, J. Magn. Magn. Mater. **52**, 18 (1985).

[14] H. Heer, A. Furrer, W. Halg, and O. Vogt, J. Phys. C **14**, L961 (1981).

[15] H. Takahashi and T. Kasuya, J. Phys. C **18**, 2697 (1985).

[16] M. Takashita, H. Aoki, C. J. Haworth, T. Matsumoto, T. Terashima, S. Uji, C. Terakura, T. Miura, A. Uesawa, and T. Suzuki, J. Phys. Soc. Jpn. **67**, 3859 (1998).

[17] M. Takashita, H. Aoki, T. Matsumoto, C. J. Haworth, T. Terashima, A. Uesawa, and T. Suzuki, Phys. Rev. Lett. **78**, 1948 (1997).

[18] It is to be noted that a magnetic moment has some possibility along the $\langle 100 \rangle$, $\langle 010 \rangle$, and $\langle 001 \rangle$ directions in a cubic NaCl crystal structure at zero magnetic field of CeSb. Once a magnetic field is applied to the CeSb system, the nearest direction to the magnetic field will be the easy magnetic axis. When the direction of magnetic field changes, especially from the $\langle 001 \rangle$ to the $\langle 100 \rangle$ direction in the (010) plane or from the $\langle 001 \rangle$ to the $\langle 110 \rangle$ direction in the (110) plane, the easy magnetic axis changes immediately to the direction of $\langle 101 \rangle$ or $\langle 111 \rangle$, respectively. Therefore, the angular dependence of the dHvA frequency shows that the discontinuous behaviors around such angles strongly depend on the direction of its easy magnetic axis.

[19] N. Môri, Y. Okayama, H. Takahashi, Y. Haga, and T. Suzuki, Jpn. J. Appl. Phys., Part 1 **8**, 182 (1983).

[20] Y. Nakanishi, F. Takahashi, T. Sakon, A. Uesawa, M. Kubota, T. Suzuki, and M. Motokawa, Physica B **281&282**, 742 (2000).

[21] T. Suzuki, Jpn. J. Appl. Phys., Part 1 **8**, 44 (1993).

[22] *Strong and Ultrastrong Magnetic Fields and their Applications*, edited by F. Herlach (Springer-Verlag, Berlin, 1983).

[23] *High Field Magnetism*, edited by F. Herlach and J. J. M. Franse (North-Holland, Amsterdam, 1989).

[24] T. Sakakibara, H. Horimoto, M. Motokawa, and M. Date, in *High Field Magnetism*, edited by M. Date (North-Holland, Amsterdam, 1983), p. 299.

[25] Y. Nakanishi *et al.*, J. Phys. Soc. Jpn. **70**, 2437 (2001).

[26] R. Settai, Ph.D. thesis, Tohoku University, 1992.

[27] B. R. Cooper and O. Vogt, J. Phys. C **1**, 1026 (1971).

[28] D. Shoenberg, *Magnetic Oscillation in Metals* (Cambridge University Press, Cambridge, England, 1984).

[29] R. G. Goodrich, N. Harrison, A. Teklu, D. Young, and Z. Fisk, Phys. Rev. Lett. **82**, 3669 (1999).

[30] A. Teklu, R. G. Goodrich, N. Harrison, D. Hall, Z. Fisk, and D. Young, Phys. Rev. B **62**, 12 875 (2000).